

Estimation of collision centrality in terms of the number of participating nucleons in heavy-ion collisions using deep learning

Dipankar Basak^{1,2} and Kalyan Dey^{1*}

^{1*}Department of Physics, Bodoland University, Kokrajhar, 783370, Assam, India.

²Department of Physics, Kokrajhar Govt. College, Kokrajhar, 783370, Assam, India.

*Corresponding author(s). E-mail(s): kalyn.dey@gmail.com;
Contributing authors: dipankar0001@gmail.com;

Abstract

The deep learning technique has been applied for the first time to investigate the possibility of centrality determination in terms of the number of participants (N_{part}) in high-energy heavy-ion collisions. For this purpose, supervised learning using both deep neural network (DNN) and convolutional neural network (CNN) is performed with labeled data obtained by modeling relativistic heavy-ion collisions utilizing A Multi-phase Transport Model (AMPT). Event-by-event distributions of pseudorapidity and azimuthal angle of charged hadrons weighted by their transverse momentum are used as input to train the DL models. The DL models did remarkably well in predicting N_{part} values with CNN slightly outperforming the DNN model. The Mean Squared Logarithmic Error (MSLE) for the CNN model (Model-4) is determined to be 0.0592 for minimum bias collisions and 0.0114 for 0-60% centrality class, indicating that the model performs better for semi-central and central collisions. Furthermore, the studied DL model is proven to be robust to changes in energy as well as model parameters of the input. The current study demonstrates that the data-driven technique has a distinct potential for determining centrality in terms of the number of participants in high-energy heavy-ion collision experiments.

Keywords: Deep learning, QGP, centrality, AMPT

1 Introduction

Investigations at various relativistic heavy-ion collision facilities suggest the formation of an extremely hot and dense state of strongly interacting matter where the quarks and gluons are no longer confined [1]. This short-lived state of matter known as Quark Gluon Plasma (QGP) is predicted to have existed barely a few microseconds after the Big Bang [2]. The favorable condition for the creation of such a hot and dense medium

formed in heavy-ion collisions depends on the produced initial energy density. If the resulting energy density surpasses $1 \text{ GeV}/\text{fm}^3$, lattice QCD predicts a phase transition from hadronic matter to deconfined QGP [3]. The production of such a hot and dense matter is only expected in head-on collisions between heavy ions at relativistic energies. In heavy-ion physics terminology, centrality is a quantity that describes the initial collision geometry and measures the amount of overlap between

the colliding nuclei. Determining centrality, therefore, becomes critical for selecting relevant events in nucleus-nucleus collisions. Geometrically, centrality can be represented by a quantity called the impact parameter¹. The total number of nucleons involved in a collision, represented by N_{part} , is another proxy for centrality in heavy-ion collisions. Unfortunately, none of the aforementioned quantities are experimentally measurable due to the femtoscopic length scale of the system. These quantities can only be determined indirectly using the Glauber model which uses experimentally measured charge particle multiplicity or the forward energy carried by the spectator nucleons as the input [4]. In the following contribution, an alternative approach based on Deep Learning has been implemented for the first time to determine collision centrality in terms of the number of participating nucleons.

The past several years have seen a rise in the use of machine learning (ML) and deep learning (DL) approaches to solve problems in a variety of modern science domains, including nuclear and high-energy physics [5–14]. DL, a subset of AI, is a very powerful data science technique capable of identifying and learning essential hidden characteristics or patterns from complex non-linear systems with high-order correlations [12]. The ML and DL models can learn pertinent attributes from data of their own without instructions being explicitly programmed. Data-driven techniques have become a useful tool for analyzing p-p, p-A, and heavy-ion physics data in parallel to conventional methods. ML and DL methods were successfully applied in the field of heavy-ion physics to determine various quantities of interest such as the impact parameter [7, 15–20], elliptic flow coefficient [21, 22], transverse sphericity [14], the temperature of the system [23] etc.

In 1996, Bass *et al.* [15] demonstrated for the first time in their study that the prediction of impact parameters using neural network approaches is considerably superior to classical methods. Among the recent works, Li *et al.* [16, 17] used ANN (Artificial Neural Network), CNN, and LightGBM (gradient-boosting machine) algorithms [24] to estimate impact parameter from

simulated Au + Au collisions at intermediate energies (0.2-1.0 GeV/nucleon) and Sn+Sn collisions at the beam energy of 270 MeV/nucleon with UrQMD model [25, 26]. The accuracy of determination of impact parameter in their study was found to be less for central collisions. Other works include the calculation of impact parameter with the help of DNN and CNN algorithms utilizing AMPT [27] generated Au+Au collisions at $\sqrt{s} = 200$ GeV [18]. Although good accuracy is observed in predicting the value of impact parameter, their model fails to achieve good accuracy for central collisions. Zhang *et al.* on the other hand using the CNN model showed reasonable accuracy in determining impact parameter throughout the entire centrality range at low-intermediate beam energies [19]. ML technique such as the Boosted Decision Trees (BDTs) [28] has been implemented by Mallick *et al.* [14] to predict impact parameter and transverse sphericity in Pb+Pb collisions at the LHC energies. Their model could able to predict both sphericity and impact parameter with Mean Absolute Error values of 0.055 and 0.52 fm respectively. On the other hand, Saha *et al.* [20] used three different standard ML algorithms namely k-nearest-neighbors (kNN), extra-trees regressor (ET), and the random forest regressor (RF) model to determine impact parameter, eccentricity, and participant eccentricity at LHC energies. Their method is found to be more accurate in determining impact parameter than the standard application of ML training methods. Another variant of deep learning models known as PointNet model [29] was applied at FAIR energies (10A GeV) to determine impact parameter on an event-by-event basis for the proposed CBM experiment [30–32]. The model was trained on features like the hit position of particles in the CBM detector planes, tracks reconstructed from the hits etc., and found to be more accurate and less model dependent than conventional methods [7].

In this present work, an attempt has been made to estimate the number of participating nucleons (N_{part}) in high-energy heavy-ion collisions with the help of a deep learning technique. The paper is structured as follows. In section 2, we discuss the methodology of the present investigation that includes event generation, a brief introduction to the AMPT model, and the input

¹Impact parameter is defined as the distance between centers of the two colliding nuclei in the plane transverse to the collision axis

selection criteria for training the studied DL models. We also presented a quick overview of the general architecture of DL models in section 3. In section 4, we presented the results where we also discussed the performance of the studied DL models with centrality, energy, input grid dimension, and on event-generator configuration. Finally, in section 5, we summarize our findings.

2 Methodology

2.1 Event Generation

A Multi-Phase Transport Model (AMPT) [27] was employed for simulating minimum bias heavy-ion collisions used as inputs for the present investigation. AMPT is a general-purpose Monte Carlo transport model used to simulate p+p, p+A, and heavy-ion collisions at relativistic energies. The model consists of four major components: initial conditions, partonic interactions, hadronization, and hadronic interactions. The initial conditions are generated according to Heavy Ion Jet Interaction Generator (HIJING) model [33], which includes the initial spatial and momentum distributions of hard minijet partons and soft string excitations. The interactions among partons are described by Zhang’s parton cascade (ZPC) model [34]. In the default version of the AMPT model, the hadronization process is implemented via the Lund string fragmentation scheme [35] and in the string melting version (AMPT-SM), it is done by the quark coalescence model [36]. Finally, the hadronic interactions are modeled via a relativistic transport model (ART) [37]. For the present study, both the versions of the AMPT model i.e. default and string melting configuration were used where minimum bias Au+Au collisions at different beam energies were generated.

2.2 Input Selection

The selection of appropriate input is critical for any DL regression task. The input variables must be chosen so that they are highly correlated with the target variable. Different kinematical parameters of the produced particles, such as transverse momentum (p_T), pseudorapidity (η), and azimuthal angle (ϕ) are expected to retain information about the initial conditions of heavy-ion collisions. Hence, for the present investigation,

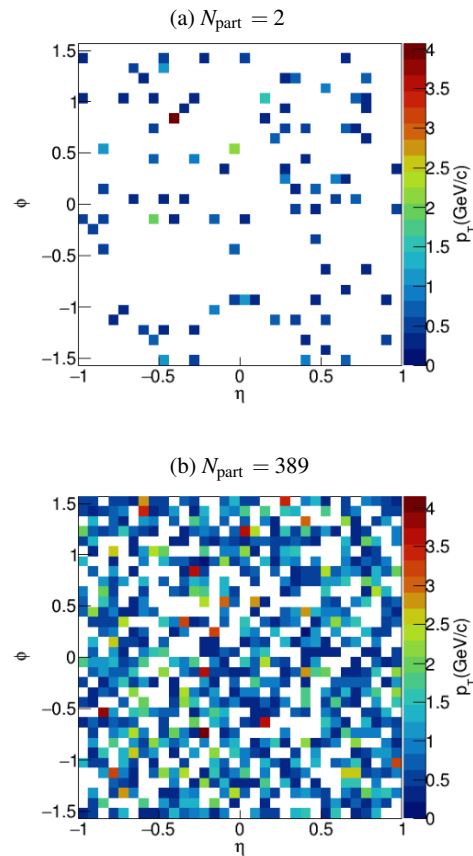


Fig. 1 (Color online) p_T weighted $(\eta - \phi)$ spectra for extreme peripheral (upper panel) with $N_{\text{part}} = 2$ and for most central (lower panel) events with $N_{\text{part}} = 389$ using AMPT-SM in Au+Au collisions at $\sqrt{s} = 200$ GeV. The spectra shown here are with 32×32 grid dimensions.

the phase space distributions of the copiously produced charged hadrons (π^\pm , k^\pm , p , \bar{p}) were considered as input to the DL models. We have used p_T weighted $(\eta - \phi)$ spectra on event-by-event basis. To mimic the realistic experimental conditions, charged hadrons within mid-rapidity ($|\eta| < 1$) acceptance which corresponds to the STAR TPC detector acceptance [38] and a transverse momentum cut of ($p_T > 0.2$ GeV/c) were chosen. In order to show two contrasting scenarios, p_T weighted $(\eta - \phi)$ spectra with 32×32 grid dimensions for both extreme central (lower panel) and most peripheral (upper panel) collisions are shown in Fig. 1.

3 Deep Learning Models

In this section, we have presented a general introduction to the DL models and discussed explicitly the architectures of different models used in the present study. Two of the most efficient DL models namely Deep Neural Networks (DNN) and Convolutional Neural Networks (CNN) are used to estimate N_{part} in high-energy heavy-ion collisions. DNN or a multilayer perceptron (MLP) is one of the simplest versions of DL models which finds application in diverse fields such as machine translation, speech recognition, and computer vision problems, just to name a few. It comprises an input layer, several hidden layers or fully-connected layers (FC), and an output layer made up of neurons or nodes. The inputs to each one of the neurons in a layer are the outputs of all of the neurons from the preceding layer. On the other hand, CNN is another powerful class of neural networks specially used for spatial pattern recognition problems. A CNN consists of several layers where the output of each layer serves as the input for the next layer. Three types of layers are generally used in a CNN model namely convolution layers, pooling layers, and fully-connected layers. The convolution layer includes kernels/filters that detect features from the input image and store the results in a so-called feature map or convolved feature. The last few layers of a CNN consist of dense layers or fully connected layers. A fully connected layer takes the inputs from the convolution layer and applies weights to predict the correct label. In addition to that, in CNNs, a pooling layer [39] is generally introduced after the convolution layers to decrease the spatial dimension of the convolution output and hence to reduce the computational complexity. Activation functions are always added with each layer to introduce non-linearity into the output of each layer. Sigmoid, tanh, and ReLU or rectified linear unit etc. are some of the commonly used activation functions. In supervised learning, the difference between the predicted output of the network and the true value is evaluated using a loss function. During the training of the neural network, the loss is minimized using an optimizer algorithm that updates the values of the parameters at every stage of the training.

The learning outcome of a DL model depends on the choice of the architecture of the model i.e.

the combinations of various hyperparameters such as the number of layers, number of pooling layers, number of fully-connected layers, the number of neurons per layer, dropout rate, learning rate, type of optimizer, etc. We checked different models with different combinations of hyperparameters values and complexity. Based on the learning performance, four DL models were finally selected for the current supervised regression task. The architecture of each of the models used in the current work is depicted in Table 1.

In all four models, for the input and hidden layers, ReLU [40] is used as the activation function while for the output layer linear activation function is considered. In all the CNN models, Average-pooling of pool size 2×2 was used as pooling layers. The most efficient Adam optimization algorithm [41] with a learning rate of 0.0001 is employed for the training of the networks and Mean-Squared Error (MSE) is chosen as the loss function. The models were allowed to train with a batch size of 64. As over-fitting is one of the common problems of any neural network, to overcome this problem we have used (i) L1 regularization [42] and L2 regularization [43], (ii) Batch normalization (BN) [44], (iii) Dropout layers [45] and (iv) EarlyStopping mechanism [46] with patience level 10. The L1 and L2 regularization prevent the weights and biases from increasing to arbitrarily large values during the optimization whereas Batch normalization normalizes the output of a layer with additional scaling and shifting, thereby increasing the rate of learning of the model by reducing the number of epochs required. EarlyStopping callback, on the other hand, is used to terminate the training process as soon as the validation error reaches its minimum value. Dropout is another popular regularization technique where some number of nodes in the layers are randomly ignored during the training process. Training of the models was performed using Keras (Version: 2.9.0) [47] with Tensorflow backend (Version: 2.9.1) [48].

4 Results and Discussions

To begin with, 180K Au+Au collisions at $\sqrt{s} = 200$ GeV were generated using AMPT-SM configuration. Out of which 30K events were kept aside for testing alone. The remaining 150K generated

Table 1 Architecture of all the DL models used in the present investigation.

Models	Model Type	Layers	Description	Total Parameters ^a
Model-1	DNN	Input	1×3072 tensor	1,737,729
		FC, ReLU	512 neurons	
		FC, ReLU	256 neurons	
		FC, ReLU	128 neurons	
		FC	1 output	
Model-2	CNN	Input	$3 \times 32 \times 32$ tensor	47,329
		Conv2D, ReLU, BN	32 kernels (3×3)	
		AveragePool2D	2×2 kernel, stride 2	
		Dropout	0.2	
		Conv2D, ReLU, BN	32 kernels (3×3)	
		AveragePool2D	2×2 kernel, stride 2	
		Dropout	0.2	
		Flatten	1152 neurons	
		FC, ReLU	32 neurons	
		FC	1 output	
		Model-3	CNN	
Conv2D, ReLU, BN	16 kernels (3×3)			
Conv2D, ReLU, BN	32 kernels (3×3)			
AveragePool2D	2×2 kernel, stride 2			
Dropout	0.2			
Conv2D, ReLU, BN	64 kernels (3×3)			
AveragePool2D	2×2 kernel, stride 2			
Dropout	0.2			
Conv2D, ReLU, BN	128 kernels (3×3)			
Dropout	0.1			
Flatten	2048 neurons			
FC, ReLU	256 neurons			
FC	1 output			
Model-4	CNN	Input	$3 \times 30 \times 30$ tensor	1,274,305
		Conv2D, ReLU, BN	32 kernels (3×3)	
		Dropout	0.2	
		Conv2D, ReLU, BN	64 kernels (3×3)	
		AveragePool2D	2×2 kernel, stride 2	
		Dropout	0.2	
		Conv2D, ReLU, BN	128 kernels (3×3)	
		AveragePool2D	2×2 kernel, stride 2	
		Dropout	0.1	
		Flatten	4608 neurons	
		FC, ReLU	256 neurons	
FC	1 output			

^aTrainable + Non-trainable parameters.

events were randomly split into training and validation data-set in the ratio of 3:1. The training

and validation learning curves for all four DL models are shown in Fig. 2. It is evident from the figure that for all four models considered in this study,

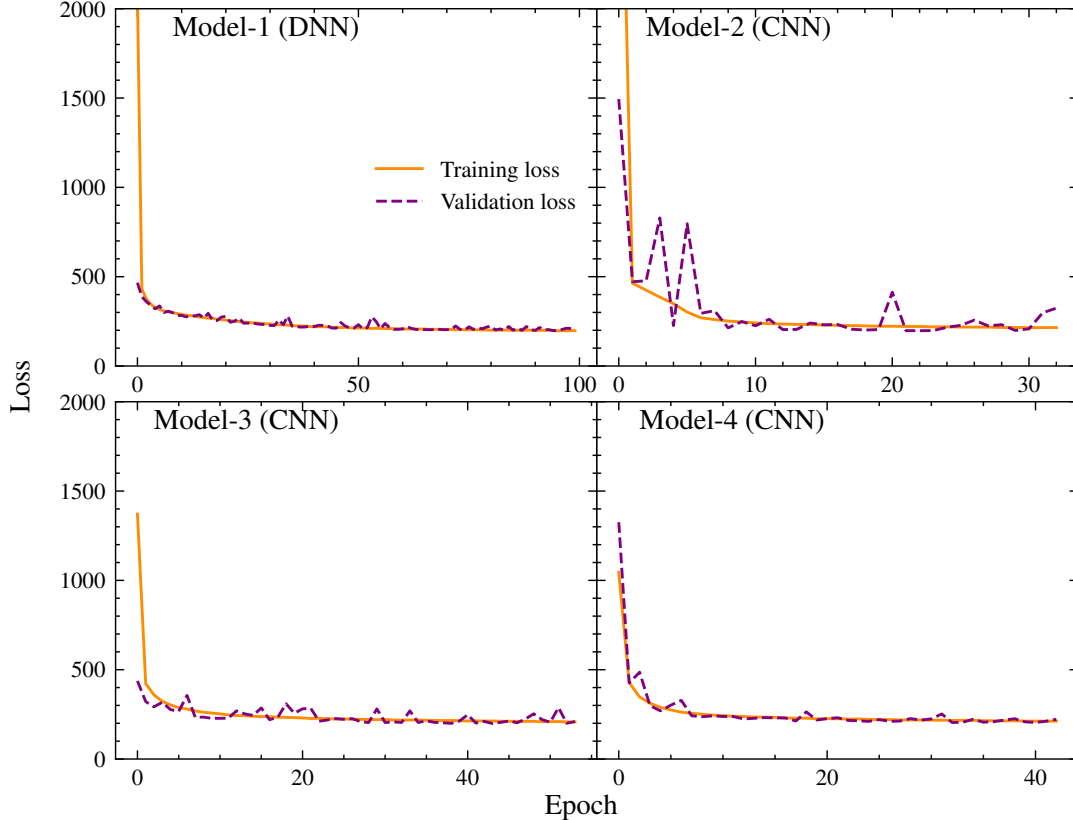


Fig. 2 (Color online) Model loss in terms of mean squared error as a function of number of epochs for all the DL models used (see text for details).

the training and validation loss decreases sharply with the number of epochs. This implied that the studied DL models are quite successful in learning hidden features from the input training data set. It is further observed from this figure that after traversing through some epochs, both the training and validation losses match roughly with each other. This indicates that the trained models generalize well in predicting the target variable using the validation data-set. The next immediate task is to check the goodness of fitting of the simulated data with the studied linear regression models. This is done by calculating R^2 -values also known as the coefficient of determination which is defined as,

$$R^2 = 1 - \frac{\sum_{i=1}^N (y_i^t - y_i^p)^2}{\sum_{i=1}^N (y_i^t - \langle y^t \rangle)^2}. \quad (1)$$

Here y and N refer to the target variable and the number of events in the test data-set respectively. y_i^t and y_i^p represent respectively the true

and predicted values of the target variable. The angular bracket $\langle \rangle$ in Eq. 1 represents the mean over all the test data samples. On average, the R^2 value is observed to be 0.98 for the studied DNN and CNN models which indicates a good fitting of the simulated data with the linear regression models. But R^2 measure alone may not determine if a regression model gives an adequate fit to the simulated data. R^2 measure in addition to the other statistical metric can provide a complete picture. The performance of the studied models has therefore been quantified using Mean Squared Logarithmic Error (MSLE) as depicted in Table 2. The expression for MSLE metric is given by,

$$\text{MSLE} = \frac{1}{N} \sum_{i=1}^N \{\log(1 + y_i^t) - \log(1 + y_i^p)\}^2. \quad (2)$$

We use MSLE as it emphasizes the relative differences between predicted and actual values, instead

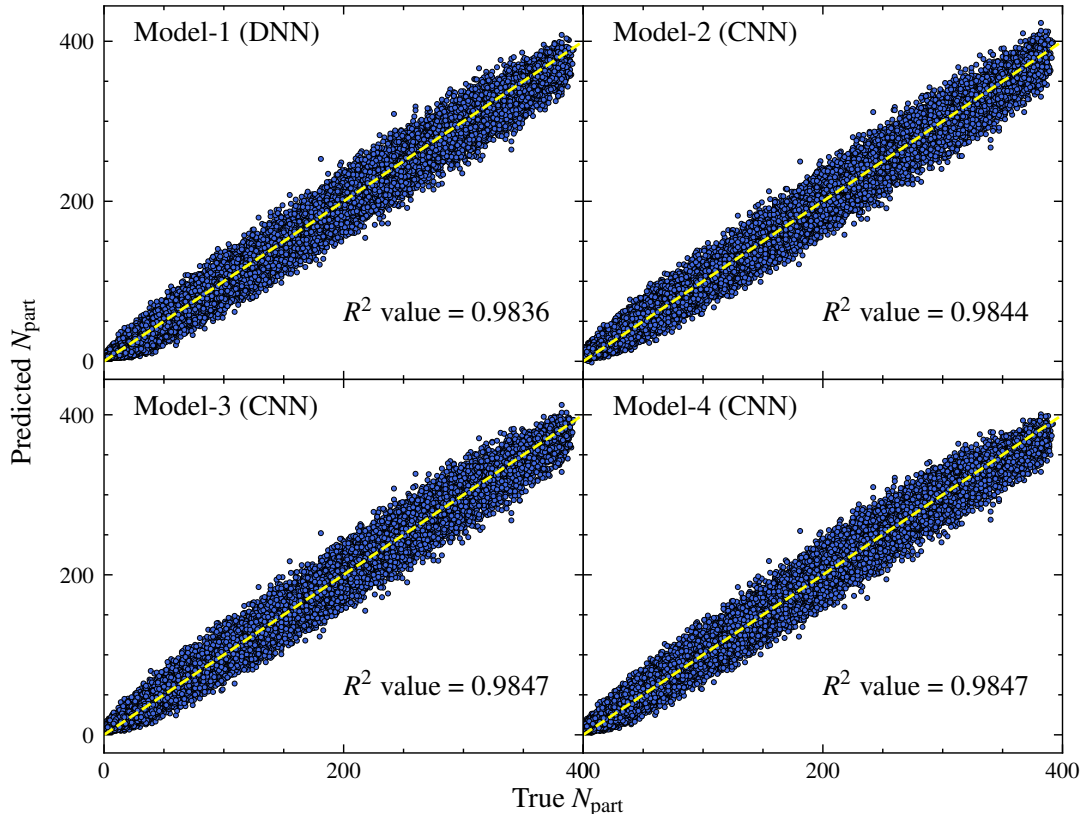


Fig. 3 (Color online) Correlation between the true and predicted N_{part} for all the DL models considered in the present study. The R^2 values are also shown.

of their absolute differences. This property is especially useful when the magnitude of the target variable varies significantly across the data-set.

Table 2 Performance of the DL models for 150 K training events and 30 K test events.

Models.	MSLE	R^2	Average Time/epoch
Model-1	0.0599	0.9836	28 sec
Model-2	0.0698	0.9844	43 sec
Model-3	0.0629	0.9847	85 sec
Model-4	0.0592	0.9847	188 sec

It is seen from Table 2, that all the DL models considered in the study have performed reasonably well in predicting N_{part} values with MSLE of about 0.06. It can further be noted that Model-4 (CNN) performs marginally better than the other models although it took a comparatively longer CPU time for execution. The large computational time taken may be due to the complexity of the

model (with around 1.2 million model parameters). It may be noted that the present DL models were not optimized for speed. The study has been performed with the help of a CPU with Intel(R) Core(TM) i5-10300H processor and 16 GB DDR4 RAM.

Fig. 3 shows the correlation plots between the true and the predicted values of the N_{part} for the DL models estimated from 30K minimum bias Au+Au collisions using AMPT-SM. The yellow dashed line corresponds to ideal prediction i.e. $N_{\text{part}}^{\text{true}} = N_{\text{part}}^{\text{pred}}$. As expected, the predicted values of N_{part} for all the DL models are well populated around the dashed lines suggesting reasonably good prediction of N_{part} by the studied DL models.

4.1 Centrality dependence

In this section, we discuss the accuracy of the DL models at different collision centralities. In order

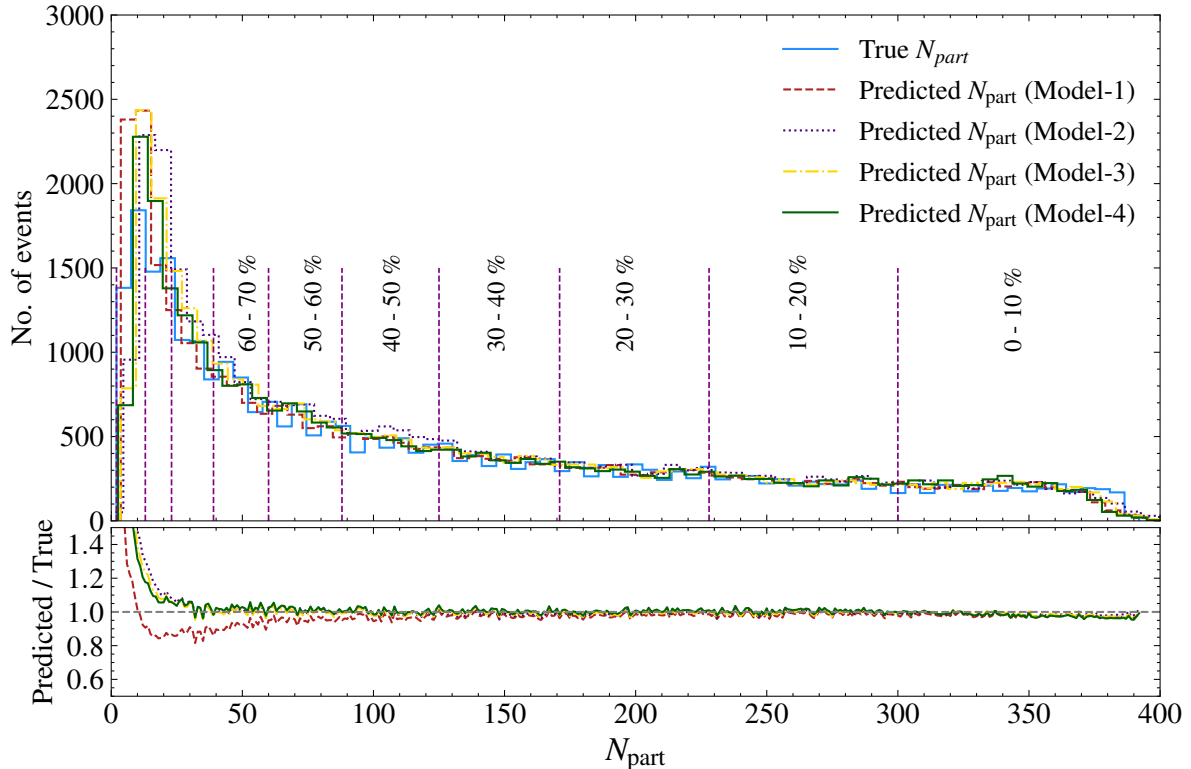


Fig. 4 (Color online) A comparison of true and predicted N_{part} distribution for the DL models. The vertical slices represent the centrality percentiles. The panel on the bottom shows the ratio of the predicted and actual N_{part} as a function of true N_{part} .

to do that the predicted N_{part} distribution is plotted for all the models and compared with the ground truth as shown in the upper panel Fig. 4. For better understanding, the ratio of predicted and true values of N_{part} is plotted against its true value as depicted in the lower panel of Fig. 4. It is seen from this figure that all the DL models perform relatively better in semi-central and central collisions while the accuracy reduces for peripheral collisions. Further, all three CNN models perform better for wider centrality range (0 – 60%) while the DNN can provide a reasonably accurate estimation of the N_{part} in a comparatively narrow centrality window (0 – 40%).

In order to quantify the accuracy of the DL models, standard metrics such as relative error and MSLE (Eq. 2) are calculated and tabulated in Table 3. The relative error is defined as,

$$\text{Relative error} = \frac{|N_{part}^t - N_{part}^p|}{N_{part}^t}. \quad (3)$$

where N_{part}^t and N_{part}^p are the true and predicted value of N_{part} respectively. The relative error in N_{part} is plotted as a function of its actual values for all the studied DL models as shown in Fig. 5. The relative error is seen to decrease sharply with the increase of N_{part} for all the DL models. From table 3, it can be seen that for all the models, the MSLE value and mean relative error (MRE) for the centrality range 0 to 60% are approximately 0.01 and 0.08 respectively while the MSLE and MRE values are higher for minimum bias collisions. The studied DL models, therefore, yield better results for semi-central and central collisions.

4.2 Input grid dimension dependence

The performance of the DL model is also examined by varying the grid dimensions of the input spectra used for training. It can be noted from the Table 4, that the performance of the DL model

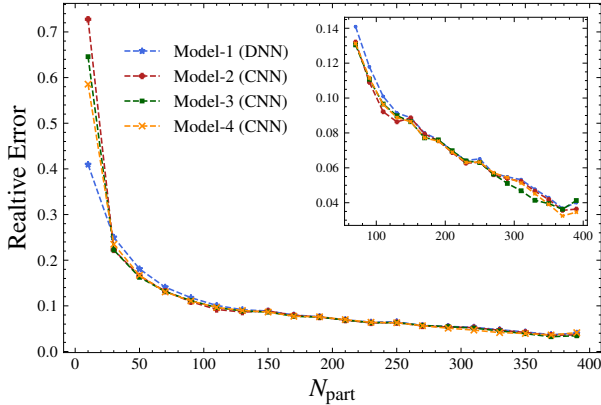


Fig. 5 (Color online) The variation of relative error against the actual value of N_{part} using the DL models. An inset plot is drawn for better visibility which magnifies the centrality window (0-60%).

Table 3 Centrality dependence of the performance of the models.

Models.	Minimum bias		0-60% centrality	
	MSLE	MRE	MSLE	MRE
Model-1	0.0599	0.1716	0.0141	0.0846
Model-2	0.0698	0.2202	0.0117	0.0809
Model-3	0.0629	0.2055	0.0118	0.0810
Model-4	0.0592	0.1970	0.0114	0.0808

(Model-4) increases with increasing grid dimension and remains virtually constant for higher grid dimensions such as 32×32 , 64×64 and 80×80 . It is also seen from Table 4, that the computational time increases exponentially with the increase of input grid dimension. Considering both factors, the entire study is being performed with grid dimensions of 32×32 .

Table 4 Performance of the CNN model (Model-4) for different grid dimensions of the inputs with $\eta - \phi$ spectra for 50K training events and 10K test events.

Grid dimension	R^2	MSLE	Average Time/epoch
16×16	0.9767	0.0700	12 sec
32×32	0.9847	0.0579	68 sec
64×64	0.9852	0.0557	311 sec
80×80	0.9840	0.0591	533 sec

Table 5 Performance of the CNN model (Model-4) for different beam energies $\sqrt{s} = 7.7, 39, 64.2, 130, 200$ GeV.

Energy (GeV)	R^2	MSLE
7.7	0.9668	0.1790
39	0.9813	0.0875
62.4	0.9815	0.0878
130	0.9829	0.0730
200	0.9842	0.0625

4.3 Energy dependence

In this section, we discuss the performance of the DL model at different beam energies. The best-performed model i.e Model-4 is used for training and testing the simulated events generated with AMPT-SM at RHIC BES (Beam Energy Scan) energies i.e. $\sqrt{s} = 7.7, 39, 62.4, 130$ GeV. For this present comparison, the DL model at all energies is trained and tested with 80K and 20K events respectively. In order to quantify the model performance, the metrics such as R^2 and MSLE values are calculated and tabulated in Table 5. Moreover, in Fig. 6, we have plotted the ratio of predicted and true N_{part} as a function of the true N_{part} values for all the energies. The model performs quite well in predicting N_{part} values at all energies as is evident from Table 5 and Fig. 6. A slight

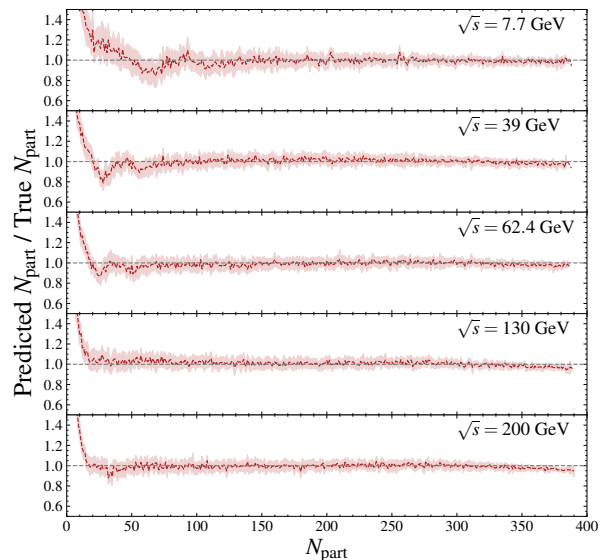


Fig. 6 (Color online) The ratio of predicted and true N_{part} as a function of true N_{part} for various beam energies such as $\sqrt{s} = 7.7, 39, 62.4, 130, 200$ GeV.

decrease in the performance is observed at the lowest beam energy i.e. $\sqrt{s} = 7.7$ GeV. Also, at all beam energies, the performance is better towards central collisions. The above two results can be explained from the fact that both at higher beam energies and at more central collisions more charged particles are produced thereby proving more information to the neural network to process for predicting N_{part} values.

4.4 Dependence on event-generator configuration

To test the robustness of the DL model against changes in the event-generator configuration, a study was conducted where the CNN model (Model-4) trained with AMPT-SM was tested with events generated with AMPT default configuration. It is to be noted that although the initial collision configuration of both AMPT-SM and AMPT default are similar, both models evolved with different physics approaches. In the default configuration, only the minijet patrons take part in ZPC and eventually recombine with parent strings by Lund string fragmentation. On the other hand, in string melting configuration, all the excited strings from the HIJING are converted into partons which increases the parton density in ZPC and hadronization takes place via the quark coalescence model. Fig. 7 shows the correlation between true and predicted N_{part} with Model-4 trained using AMPT-SM but tested with

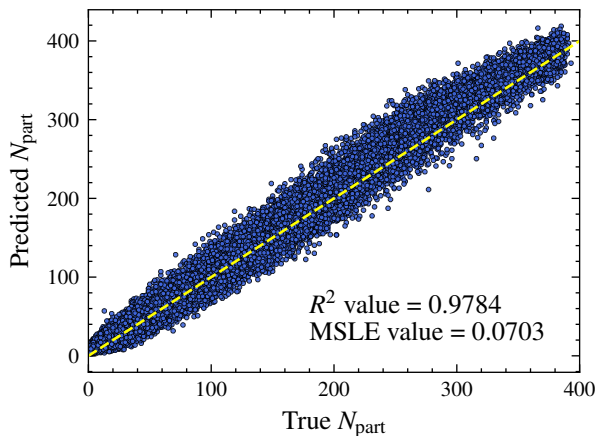


Fig. 7 (Color online) Correlation between the true and predicted N_{part} with Model-4 trained using AMPT-SM but tested with AMPT default events.

AMPT default events. The R^2 and MSLE values of the prediction are found to be 0.9784 and 0.0703 respectively from which it is clear that in spite of the differences in physics perspective for both the AMPT-SM and AMPT default models, the present DL model could able to generalize well in predicting N_{part} values for the AMPT default configuration.

5 Summary

The deep learning technique has been employed for the first time to determine centrality in terms of N_{part} in high-energy heavy-ion collisions. For this study, we have used two variants of DL models such as DNN and CNN. p_T weighted $(\eta - \phi)$ spectra of charged hadrons produced in minimum bias Au+Au collisions at $\sqrt{s} = 200$ GeV generated with AMPT-SM model were used to train the DL models. Although the studied DL models did perform remarkably well in estimating N_{part} , especially for semi-central and central collisions, the CNN provides marginally better results. To cross-check the performance of the DL model at other energies, the best-performing model (model-4) without altering its architecture was trained and tested at different RHIC-BES energies, namely $\sqrt{s} = 7.7, 39, 64.2, 130$ GeV. Except for the lowest beam energy, the performance of the DL model at other energies is identical to that of the top RHIC energy i.e. $\sqrt{s} = 200$ GeV as demonstrated by the R^2 and MSLE values. Further, the efficacy of the studied DL model is also investigated by changing the event-generator configuration. The DL model (model-4) trained using AMPT-SM is therefore tested with the AMPT default configuration and predicts N_{part} values with reasonable accuracy, indicating that the studied DL model is robust to changes in event-generator configuration.

References

- [1] An overview of star experimental results. Nuclear Physics A **931**, 1–12 (2014). <https://doi.org/10.1016/j.nuclphysa.2014.10.022>. Quark Matter 2014
- [2] Studying the early universe via quark-gluon plasma. Nuclear Physics B - Proceedings Supplements **246-247**, 38–41 (2014). <https://doi.org/10.1016/j.nuclphysbps.2013>.

- 10.063. Proceedings of the 9th International Symposium on Cosmology and Particle Astrophysics
- [3] Lattice results on qcd thermodynamics. Nuclear Physics A **698**(1), 199–208 (2002). [https://doi.org/10.1016/S0375-9474\(01\)01365-3](https://doi.org/10.1016/S0375-9474(01)01365-3). 15th Int. Conf. on Ultra-Relativistic Nucleus-Nucleus Collisions (Quark Matter 2001)
- [4] M.L. Miller, K. Reygers, S.J. Sanders, P. Steinberg, Glauber modeling in high-energy nuclear collisions. Annual Review of Nuclear and Particle Science **57**(1), 205–243 (2007). <https://doi.org/10.1146/annurev.nucl.57.090506.123020>
- [5] A. Boehnlein, et al., Colloquium: Machine learning in nuclear physics. Rev. Mod. Phys. **94**, 031003 (2022). <https://doi.org/10.1103/RevModPhys.94.031003>
- [6] Y.L. Du, K. Zhou, J. Steinheimer, L.G. Pang, A. Motornenko, H.S. Zong, X.N. Wang, H. Stöcker, Identifying the nature of the QCD transition in relativistic collision of heavy nuclei with deep learning. Eur. Phys. J. C **80**(6), 516 (2020). <https://doi.org/10.1140/epjc/s10052-020-8030-7>. arXiv:1910.11530 [hep-ph]
- [7] M.O. Kuttan, K. Zhou, J. Steinheimer, A. Redelbach, H. Stoecker, An equation-of-state-meter for CBM using PointNet [https://doi.org/10.1007/jhep10\(2021\)184](https://doi.org/10.1007/jhep10(2021)184)
- [8] Y.S. Zhao, L. Wang, K. Zhou, X.G. Huang, Detecting the chiral magnetic effect via deep learning. Phys. Rev. C **106**, L051901 (2022). <https://doi.org/10.1103/PhysRevC.106.L051901>
- [9] G. Bíró, B. Tankó-Bartalis, G.G. Barnaföldi. Studying Hadronization by Machine Learning Techniques (2021). URL <https://arxiv.org/abs/2111.15655>
- [10] J.W. Monk, Deep learning as a parton shower. Journal of High Energy Physics **2018**(10), 21 (2018). [https://doi.org/10.1007/jhep12\(2018\)021](https://doi.org/10.1007/jhep12(2018)021)
- [11] E. Shokr, A. De Roeck, M. Mahmoud, Modeling of charged-particle multiplicity and transverse-momentum distributions in pp collisions using a dnn. Scientific Reports **12** (2022). <https://doi.org/10.1038/s41598-022-11618-6>
- [12] L.G. Pang, K. Zhou, N. Su, H. Petersen, H. Stöcker, X.N. Wang, An equation-of-state-meter of quantum chromodynamics transition from deep learning. Nature Communications **9**(1), 210 (2018). <https://doi.org/10.1038/s41467-017-02726-3>
- [13] C.Y. Tsang, et al., Applying machine learning to determine impact parameter in nuclear physics experiments (2021). arXiv:2107.13985 [physics.ins-det]
- [14] N. Mallick, S. Tripathy, A.N. Mishra, S. Deb, R. Sahoo, Estimation of impact parameter and transverse sphericity in heavy-ion collisions at the lhc energies using machine learning. Phys. Rev. D **103**, 094031 (2021). <https://doi.org/10.1103/PhysRevD.103.094031>
- [15] S.A. Bass, A. Bischoff, J.A. Maruhn, H. Stöcker, W. Greiner, Neural networks for impact parameter determination. Phys. Rev. C **53**, 2358–2363 (1996). <https://doi.org/10.1103/PhysRevC.53.2358>
- [16] F. Li, Y. Wang, H. Lü, L. Cheng, Q. Li, F. Liu, Application of artificial intelligence in the determination of impact parameter in heavy-ion collisions at intermediate energies. Journal of Physics G: Nuclear and Particle Physics **47** (2020). <https://doi.org/10.1088/1361-6471/abb1f9>
- [17] F. Li, Y. Wang, Z. Gao, P. Li, H. Lü, Q. Li, C.Y. Tsang, M.B. Tsang, Application of machine learning in the determination of impact parameter in the $^{132}\text{Sn} + ^{124}\text{Sn}$ system. Phys. Rev. C **104**, 034608 (2021). <https://doi.org/10.1103/PhysRevC.104.034608>
- [18] P. Xiang, Y.S. Zhao, X.G. Huang, Determination of the impact parameter in high-energy heavy-ion collisions via deep learning. Chinese Physics C **46**(7), 074110 (2022). <https://doi.org/10.1088/1674-1137/ac6490>

- [19] X. Zhang, X. Liu, et al., Determining impact parameters of heavy-ion collisions at low-intermediate incident energies using deep learning with convolutional neural networks. *Phys. Rev. C* **105**, 034611 (2022). <https://doi.org/10.1103/PhysRevC.105.034611>
- [20] A. Saha, D. Dan, S. Sanyal, Machine-learning model-driven prediction of the initial geometry in heavy-ion collision experiments. *Phys. Rev. C* **106**, 014901 (2022). <https://doi.org/10.1103/PhysRevC.106.014901>
- [21] N. Mallick, S. Prasad, A.N. Mishra, R. Sahoo, G.G. Barnaföldi, Estimating elliptic flow coefficient in heavy ion collisions using deep learning. *Phys. Rev. D* **105**, 114022 (2022). <https://doi.org/10.1103/PhysRevD.105.114022>
- [22] N. Mallick, S. Prasad, A.N. Mishra, R. Sahoo, G.G. Barnaföldi, Deep learning predicted elliptic flow of identified particles in heavy-ion collisions at the RHIC and LHC energies (2023). [arXiv:2301.10426](https://arxiv.org/abs/2301.10426) [hep-ph]
- [23] Determining the temperature in heavy-ion collisions with multiplicity distribution. *Physics Letters B* **814**, 136084 (2021). <https://doi.org/10.1016/j.physletb.2021.136084>
- [24] G. Ke, Q. Meng, T. Finley, T. Wang, W. Chen, W. Ma, Q. Ye, T.Y. Liu, in *Advances in Neural Information Processing Systems*, vol. 30, ed. by I. Guyon, U.V. Luxburg, S. Bengio, H. Wallach, R. Fergus, S. Vishwanathan, R. Garnett (Curran Associates, Inc., 2017). URL <https://papers.nips.cc/paper/2017/hash/6449f44a102fde848669bdd9eb6b76fa-Abstract.html>
- [25] S. Bass, et al., Microscopic models for ultrarelativistic heavy ion collisions. *Progress in Particle and Nuclear Physics* **41**, 255–369 (1998). [https://doi.org/10.1016/s0146-6410\(98\)00058-1](https://doi.org/10.1016/s0146-6410(98)00058-1)
- [26] M. Bleicher, E. Zabrodin, C. Spieles, S.A. Bass, C. Ernst, S. Soff, L. Bravina, M. Belkacem, H. Weber, H. Stöcker, W. Greiner, Relativistic hadron-hadron collisions in the ultra-relativistic quantum molecular dynamics model. *Journal of Physics G: Nuclear and Particle Physics* **25**(9), 1859–1896 (1999). <https://doi.org/10.1088/0954-3899/25/9/308>
- [27] Z.W. Lin, C.M. Ko, B.A. Li, B. Zhang, S. Pal, Multiphase transport model for relativistic heavy ion collisions. *Phys. Rev. C* **72**, 064901 (2005). <https://doi.org/10.1103/PhysRevC.72.064901>
- [28] J.H. Friedman, Greedy function approximation: A gradient boosting machine. *The Annals of Statistics* **29**(5), 1189 – 1232 (2001). <https://doi.org/10.1214/aos/1013203451>
- [29] C.R. Qi, H. Su, K. Mo, L.J. Guibas. Pointnet: Deep learning on point sets for 3d classification and segmentation (2016). <https://doi.org/10.48550/ARXIV.1612.00593>
- [30] T. Ablyazimov, A. Abuhoza, et al., Challenges in QCD matter physics –the scientific programme of the compressed baryonic matter experiment at FAIR. *The European Physical Journal A* **53**(3), 60 (2017). <https://doi.org/10.1140/epja/i2017-12248-y>
- [31] P. Senger, Astrophysics in the laboratory—the CBM experiment at FAIR. *Particles* **3**(2), 320–335 (2020). <https://doi.org/10.3390/particles3020024>
- [32] C. and Höhne, The cbm experiment at fair exploring the qcd phase diagram at high net baryon densities. *International Journal of Modern Physics E* **16**(07n08), 2419–2424 (2007). <https://doi.org/10.1142/S0218301307008033>
- [33] X.N. Wang, M. Gyulassy, hijing: A monte carlo model for multiple jet production in pp, pA, and AA collisions. *Phys. Rev. D* **44**, 3501–3516 (1991). <https://doi.org/10.1103/PhysRevD.44.3501>
- [34] Zpc 1.0.1: a parton cascade for ultrarelativistic heavy ion collisions. *Computer Physics Communications* **109**(2), 193–206 (1998). [https://doi.org/10.1016/S0010-4655\(98\)00000-1](https://doi.org/10.1016/S0010-4655(98)00000-1)

00010-1

- [35] Parton fragmentation and string dynamics. *Physics Reports* **97**(2), 31–145 (1983). [https://doi.org/10.1016/0370-1573\(83\)90080-7](https://doi.org/10.1016/0370-1573(83)90080-7)
- [36] Y. He, Z.W. Lin, Improved quark coalescence for a multi-phase transport model. *Phys. Rev. C* **96**, 014910 (2017). <https://doi.org/10.1103/PhysRevC.96.014910>
- [37] B.A. Li, C.M. Ko, Formation of superdense hadronic matter in high energy heavy-ion collisions. *Phys. Rev. C* **52**, 2037–2063 (1995). <https://doi.org/10.1103/PhysRevC.52.2037>
- [38] The star time projection chamber: a unique tool for studying high multiplicity events at rhic. *Nuclear Instruments and Methods in Physics Research Section A: Accelerators, Spectrometers, Detectors and Associated Equipment* **499**(2), 659–678 (2003). [https://doi.org/10.1016/S0168-9002\(02\)01964-2](https://doi.org/10.1016/S0168-9002(02)01964-2). The Relativistic Heavy Ion Collider Project: RHIC and its Detectors
- [39] D. Scherer, A. Müller, S. Behnke, in *Artificial Neural Networks – ICANN 2010*, ed. by K. Diamantaras, W. Duch, L.S. Iliadis (Springer Berlin Heidelberg, Berlin, Heidelberg, 2010), pp. 92–101. https://doi.org/10.1007/978-3-642-15825-4_10
- [40] V. Nair, G.E. Hinton, in *Proceedings of the 27th International Conference on International Conference on Machine Learning* (Omnipress, Madison, WI, USA, 2010), ICML’10, p. 807–814. URL <https://dl.acm.org/doi/10.5555/3104322.3104425>
- [41] D.P. Kingma, J. Ba, Adam: A method for stochastic optimization. *CoRR abs/1412.6980* (2014). <https://doi.org/10.48550/arXiv.1412.6980>
- [42] R. Tibshirani, Regression shrinkage and selection via the lasso. *Journal of the Royal Statistical Society: Series B (Methodological)* **58**(1), 267–288 (1996). <https://doi.org/10.1111/j.2517-6161.1996.tb02080.x>
- [43] G.E. Hinton, in *Proceedings of the eighth annual conference of the cognitive science society* (Amherst, MA, 1986), pp. 1–12
- [44] S. Ioffe, C. Szegedy, in *Proceedings of the 32nd International Conference on Machine Learning, Proceedings of Machine Learning Research*, vol. 37, ed. by F. Bach, D. Blei (PMLR, Lille, France, 2015), pp. 448–456. URL <https://proceedings.mlr.press/v37/ioffe15.html>
- [45] N. Srivastava, G. Hinton, A. Krizhevsky, I. Sutskever, R. Salakhutdinov, Dropout: A simple way to prevent neural networks from overfitting. *Journal of Machine Learning Research* **15**(56), 1929–1958 (2014). URL <http://jmlr.org/papers/v15/srivastava14a.html>
- [46] Y. Yao, L. Rosasco, A. Caponnetto, On early stopping in gradient descent learning. *Constructive Approximation* **26**(2), 289–315 (2007). <https://doi.org/10.1007/s00365-006-0663-2>
- [47] F. Chollet, et al. <https://keras.io/>
- [48] M. Abadi, et al., in *Proceedings of the 12th USENIX Conference on Operating Systems Design and Implementation* (USENIX Association, USA, 2016), OSDI’16, p. 265–283. URL <https://dl.acm.org/doi/10.5555/3026877.3026899>